Supporting Information for "Electrokinetic contributions to self-potential signals from magmatic stressing"

Fee Arens[1], Joachim Gottsmann[1], Karen Strehlow[2], James Hickey[3], and Geoff Kilgour[4]

[1]School of Earth Sciences, University of Bristol, Bristol, UK

[2]GEOMAR Helmholtz Centre for Ocean Research Kiel, Germany

[3]Camborne School of Mines, University of Exeter, Cornwall, UK

[4]GNS Science, Wairakei Research Centre, Taupo, New Zealand

Contents of this file

Introduction

Enclosed are supplementary model boundary conditions and their influence on SP signals at the surface, as well as additional model results for the reference simulations and a comparison between elasticity and poroelasticity.

Model boundary conditions

Corresponding author: Fee Arens, fee.arens@bristol.ac.uk

All results presented in this study are conditional on the applied boundary conditions. Changing those conditions will change the results. For example, a no-flow boundary condition in the cap rock by assigning zero permeability prevents fluid flow and electrokinetic processes (in line with the study of Revil et al. (2008)). As a consequence, the SP signals at the surface are generated exclusively by pore pressure variations and groundwater flow in the aquifer. Excluding electrokinetic processes in the cap rock in our study substantially modifies the SP signal for the initial response as shown in Figure S3 for both dike and sill models. While the PA no-flow model exhibits a reversed SP pattern relative to the reference model, the LFA model varies only in magnitude and polarity. This contrasting behaviour underlines the lithological control on the SP signal. Temporal SP signals at the central point at the ground surface (x = z = 0) shows markedly differences between the no-flow and benchmark models, except for the LFA dike model where only magnitude varies. SP signals in the PA dike model show initial variations between both models, but stabilize around the same value, indicating that SP signal with time is dominated by processes in the aquifer in the reference model. Temporal SP differences between the no-flow and the reference models are mainly due to fluid flow dynamics controlled by domain properties.

References

Revil, A., Finizola, A., Piscitelli, S., Rizzo, E., Ricci, T., Crespy, A., ... Suski, B. (2008). Inner structure of La Fossa di Vulcano (Vulcano Island, southern Tyrrhenian Sea, Italy) revealed by high-resolution electric resistivity tomography coupled with self-potential, temperature, and CO2 diffuse degassing measurements. *Journal of Geophysical Research: Solid Earth*, *113*(7), 1–21. doi: 10.1029/2007JB005394

Table S1. Overview of temperature-dependent fluid properties.

	Temperature (°C)						
Parameter	5	10	25	50	75	100	200
PA model							
ρ_{aq} (kg m^{-3})	1005.4	10004.9	1001.99	992.8	979.7	963.48	871.8
η_{aq} (Pa s)	$1.50{\cdot}10^{-3}$	$1.3{\cdot}10^{-3}$	$8.9{\cdot}10^{-4}$	$5.49{\cdot}10^{-4}$	$3.81{\cdot}10^{-4}$	$2.85{\cdot}10^{-4}$	$1.37{\cdot}10^{-4}$
χ_{aq} (Pa^{-1})	$4.77{\cdot}10^{-10}$	$4.64{\cdot}10^{-10}$	$4.4{\cdot}10^{-10}$	$4.28{\cdot}10^{-10}$	$4.41{\cdot}10^{-10}$	$4.72{\cdot}10^{-10}$	$8.24{\cdot}10^{-10}$
ρ_c(kg m^{-3})	1001.7	1001.4	998.7	989.6	976.4	960	866.3
η_c (Pa s)	$1.5{\cdot}10^{-3}$	$1.3{\cdot}10^{-3}$	$8.89{\cdot}10^{-4}$	$5.47{\cdot}10^{-4}$	$3.8{\cdot}10^{-4}$	$2.8{\cdot}10^{-4}$	$1.3{\cdot}10^{-4}$
χ_c (Pa^{-1})	$4.87{\cdot}10^{-10}$	$4.74{\cdot}10^{-10}$	$4.48{\cdot}10^{-10}$	$4.3{\cdot}10^{-10}$	$4.5{\cdot}10^{-10}$	$4.83{\cdot}10^{-10}$	$8.7{\cdot}10^{-10}$
LFA model							
ρ_{aq}(kg m^{-3})	1009.2	1008.7	1005.5	996.5	983.2	967.1	887.5
η_{aq} (Pa s)	$1.5{\cdot}10^{-3}$	$1.3{\cdot}10^{-3}$	$8.9{\cdot}10^{-4}$	$5.5{\cdot}10^{-4}$	$3.8{\cdot}10^{-4}$	$2.9{\cdot}10^{-4}$	$1.4{\cdot}10^{-4}$
χ_{aq} (Pa^{-1})	$4.86{\cdot}10^{-10}$	$4.55{\cdot}10^{-10}$	$4.31{\cdot}10^{-10}$	$4.2{\cdot}10^{-10}$	$4.31{\cdot}10^{-10}$	$4.6{\cdot}10^{-10}$	$7.81{\cdot}10^{-10}$
ρ_c (kg m^{-3})	1003.0	1002.7	999.9	990.8	977.6	961.3	868.3
η_c (Pa s)	$1.5{\cdot}10^{-3}$	$1.3{\cdot}10^{-3}$	$5.4{\cdot}10^{-4}$	$5.4{\cdot}10^{-4}$	$3.8{\cdot}10^{-4}$	$2.8{\cdot}10^{-4}$	$1.4{\cdot}10^{-4}$
χ_c (Pa^{-1})	$4.83{\cdot}10^{-10}$	$4.7{\cdot}10^{-10}$	$4.45{\cdot}10^{-10}$	$4.33{\cdot}10^{-10}$	$4.47{\cdot}10^{-10}$	$4.48{\cdot}10^{-10}$	$4.85{\cdot}10^{-10}$

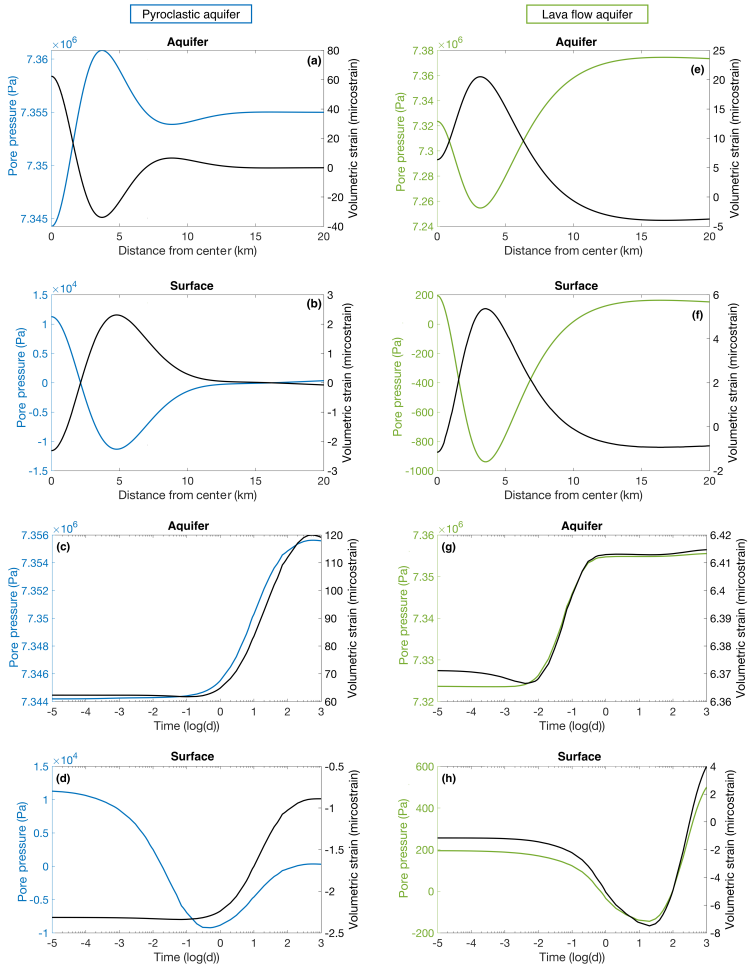

Figure S1. Overview of pore pressure (p_f) and volumetric strain (ϵ_{vol}) with distance (a,b,e,f) and time (c,d,g,h) at the surface (z = 0) and in the aquifer (z = -0.75 km). In the PA model p_f and ϵ_{vol} show a contrasting behavior in the aquifer (a) and at the surface (b), while in the LFA model similar spatial patterns can be observed in both domains (e-f). Positive volumetric strain (dilation) relates to a fall in pore pressure. Differences in the spatial pattern of p_f and ϵ_{vol} depend on the elastic stratigraphy of the models. In the PA model p_f and ϵ_{vol} increase in the aquifer (c) and at the surface (d) with time. In the lava flow aquifer p_f and ϵ_{vol} increase rapidly followed by a phase of stabilisation at log(d)$\sim$3 (g). At the surface both signals vary throughout time (h).

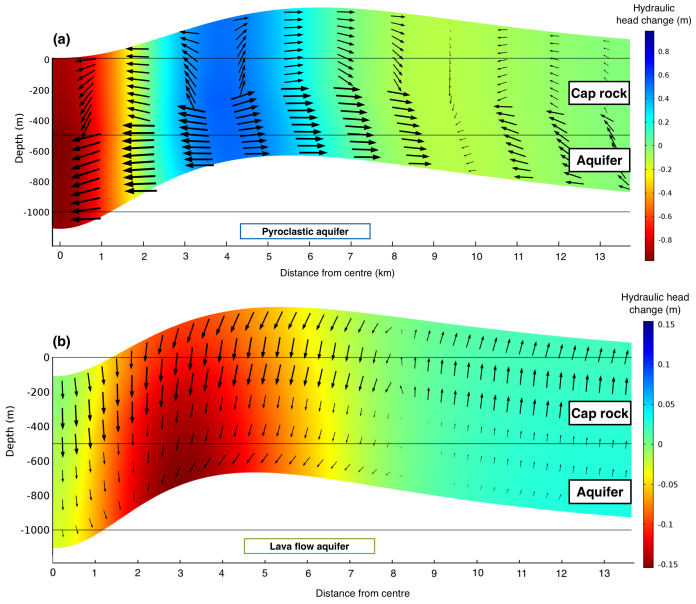

Figure S2. 2D overview of fluid flow (arrow surface), hydraulic head change (colouring) and deformation in the cap rock and the aquifer for (a) PA and (b) LFA model at t = 1 d. Note that as shown, the displacements are not to scale and given only for representation purposes; a central subsidence and vertical uplift ∼4 - 5 km is observed in both models. Background boxes (black) represent undeformed domain conditions prior to source pressurisation. Fluid flow shows a distinguishable pattern between both model setups. Arrows indicate the flow direction, while their length is related logarithmic to the fluid velocity with different scales for (a) and (b). In the PA model, fluid points away from area of uplift (∼ 4 - 5 km) towards central subsidence. In the LFA model, fluid flows predominantly downwards from cap rock to aquifer (<8 km from the centre), while in the aquifer water flows towards the area of uplift, accumulating at the bottom of the slope. Hydraulic head changes (ΔH) are relative to vertical displacement (v; as ΔH-v) and reflect pore pressure variations. In both models, a subsidence above the dike induces a central fall in head height. Vertical uplift (∼4 - 5 km) provokes a rise in water tables in the PA model but a fall in the LFA model, governed by the elastic properties of the subsurface.

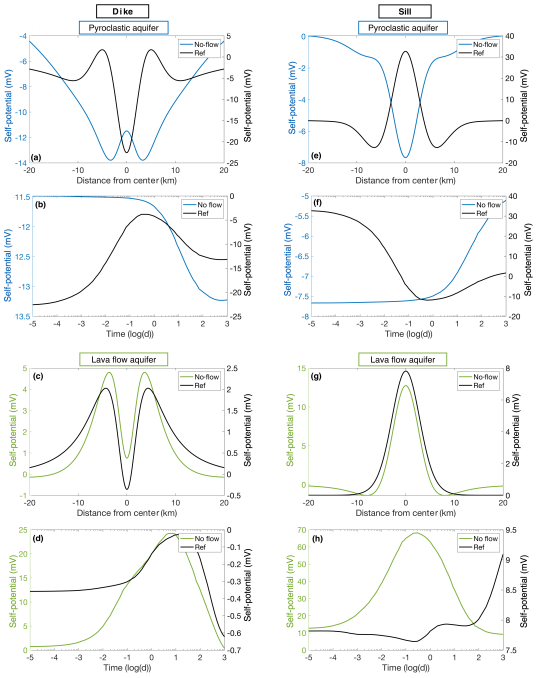

Figure S3. Comparison of SP anomalies between no-flow cap rock boundary conditions (green/blue) and the reference model (black). The no-flow condition is implemented by assigning zero permeability to the cap rock disabling electrokinetic processes. Hence SP anomalies at the surface are produced exclusively by fluid processes in the aquifers in the no-flow model. The superficial SP pattern for t = 1 s after source pressurization is displayed for (a) PA, (c) LFA model for a dike and (e) PA and (g) LFA model for a sill. SP signals in the PA model show greatest deviations between no-flow and reference model, with an inverse spatial pattern. Within the LFA model, only SP magnitude varies between both models, while the spatial footprint is similar. Streaming potential with time (log-scale) is shown at the superficial central point (x = z = 0). SP signals from the no-flow simulations show similar temporal evolution relative to the reference model in the PA model for (b) dike and (f) sill pressurization, as well as dike LFA model (d). The temporal SP pattern in the LFA varies substantially between no-flow and reference models for the case of a pressurized sill (h).

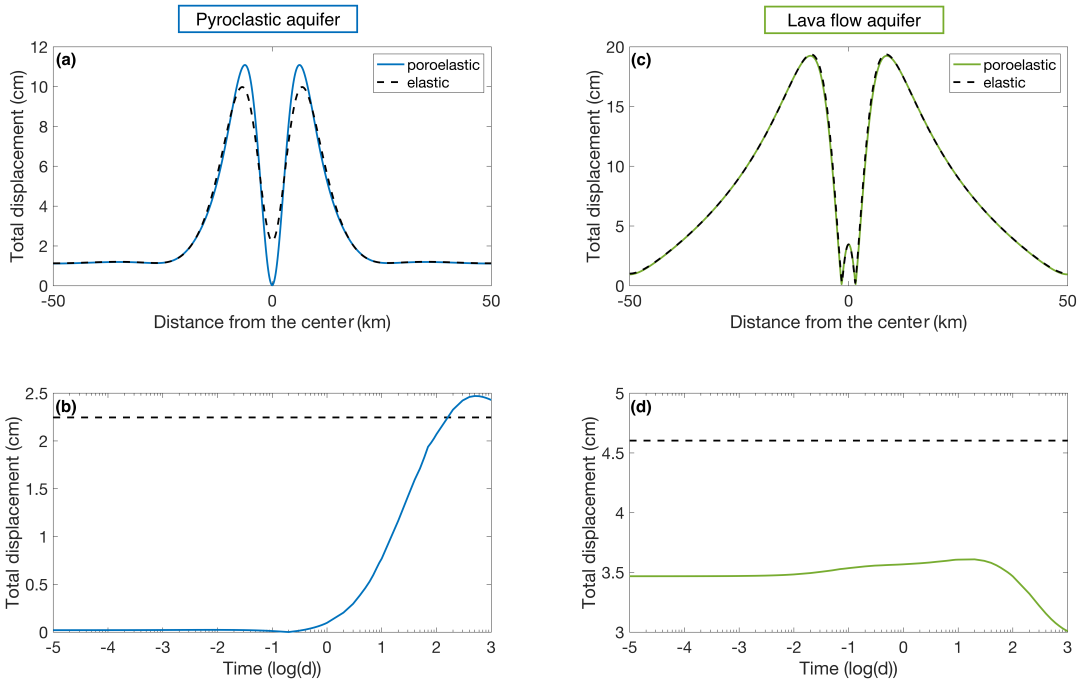

Figure S4. Total displacement at the ground surface for a purely linear elastic (black) vs poroelastic crust. Upper panels show the deformation along the free surface at t=1s after the dike pressurization for (a) the PA and (c) the LFA models. Results show that the poroelastic response markedly influences the deformation pattern in the PA model compared to its elastic solution, while the LFA model only shows on minor deviations. Lower panels display the deformation time series (log-scale) at the central superficial point (x = z = 0) for (b) the PA and (d) the LFA models. While the elastic solution remains constant over time (as expected), the poroelastic response modulates the displacement field with time.